

Supporting Information

Manuscript number: ejic.202200478

Contents	Page
Figure S1. HRMS ESI ⁺ : experimental (top) and simulated (bottom) ion peaks of compound 2 .	2
Figure S2. HRMS ESI ⁺ : experimental (top) and simulated (bottom) ion peaks of bimetallic complex 3 .	2
Figure S3. HRMS ESI ⁺ : experimental (top) and simulated (bottom) ion peaks of bimetallic complex 4 .	3
Figure S4. HRMS ESI ⁺ : experimental (top) and simulated (bottom) ion peaks of bimetallic complex 5 .	3
Figure S5. HRMS ESI ⁺ : experimental (top) and simulated (bottom) ion peaks of bimetallic complex 6 .	3
Figure S6. FT-IR solid-state spectrum (KBr disk) of metalloligand 2 .	4
Figure S7. FT-IR solid-state spectrum (KBr disk) of bimetallic complex 3 .	4
Figure S8. FT-IR solid-state spectrum (KBr disk) of bimetallic complex 4 .	5
Figure S9. FT-IR solid-state spectrum (KBr disk) of bimetallic complex 5 .	5
Figure S10. FT-IR solid-state spectrum (KBr disk) of bimetallic complex 6 .	6
Figure S11. ¹ H NMR spectrum of the bimetallic complex 3 recorded in DMSO- <i>d</i> ₆ at 298 K.	6
Figure S12. ¹ H NMR spectrum of the bimetallic complex 5 recorded in DMSO- <i>d</i> ₆ at 298 K.	7
Figure S13. ¹³ C{ ¹ H} NMR spectrum of the metalloligand 2 recorded in DMSO- <i>d</i> ₆ at 298 K.	7
Figure S14. ¹³ C{ ¹ H} NMR spectrum of the bimetallic complex 3 recorded in DMSO- <i>d</i> ₆ at 298 K.	8
Figure S15. ¹³ C{ ¹ H} NMR spectrum of the bimetallic complex 5 recorded in DMSO- <i>d</i> ₆ at 298 K.	8
Figure S16. ¹³ C{ ¹ H} NMR spectrum of the bimetallic complex 6 recorded in DMSO- <i>d</i> ₆ at 298 K.	9
Figure S17. Packing diagram of complex 2 showing the molecular arrangement and hydrogen-bond interactions.	10
Figure S18. Packing diagram of bimetallic complex 3 showing the molecular arrangement and hydrogen-bond interactions.	11
Figure S19. UV-vis spectra of complexes 4 (top) and 5 (bottom) recorded in DCM (black line) and DMF (blue line) solutions.	12
Figure S20. The linear correlation between the electrochemical $E_{1/2}$ and the computed ionization energies of complexes 2 , 3 , 4 and 5 . Complex 6 is added for comparison.	12
Figure S21. TD-DFT-simulated UV-vis spectra of complexes 2-6 .	13

Figure S22. The TD-DFT-simulated UV-vis spectra of complex **2** in vacuum (red curve) and in DMF (black curve) 13

Table S1. Selected bond distances (Å) and angles (°) for compounds **2** and **3**. 14

Table S2. Selected metrical parameters of the ferrocenyl units in compounds **2** and **3**. 14

Table S3. Intra- and intermolecular hydrogen bond interactions in metalloligand **2**. 15

Table S4. Intermolecular hydrogen bond interactions in complex **3**. 15

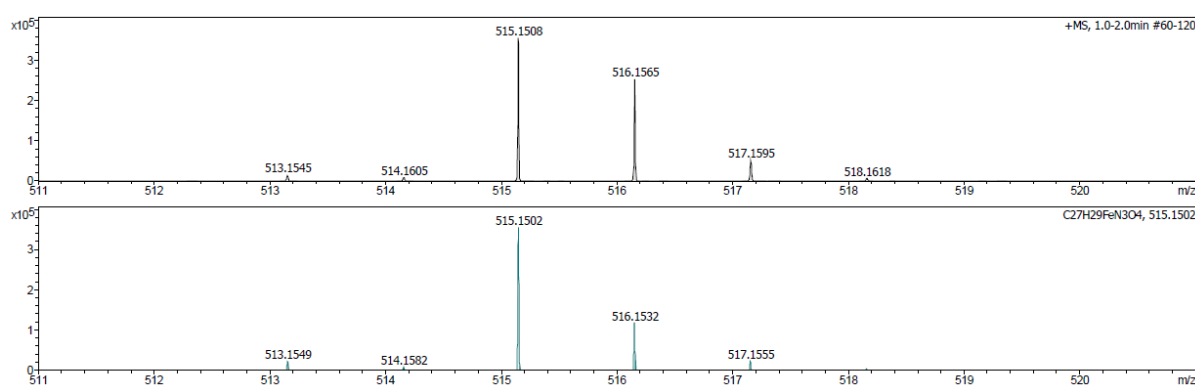


Figure S1. HRMS ESI⁺: experimental (top) and simulated (bottom) ion peaks of compound **2**.

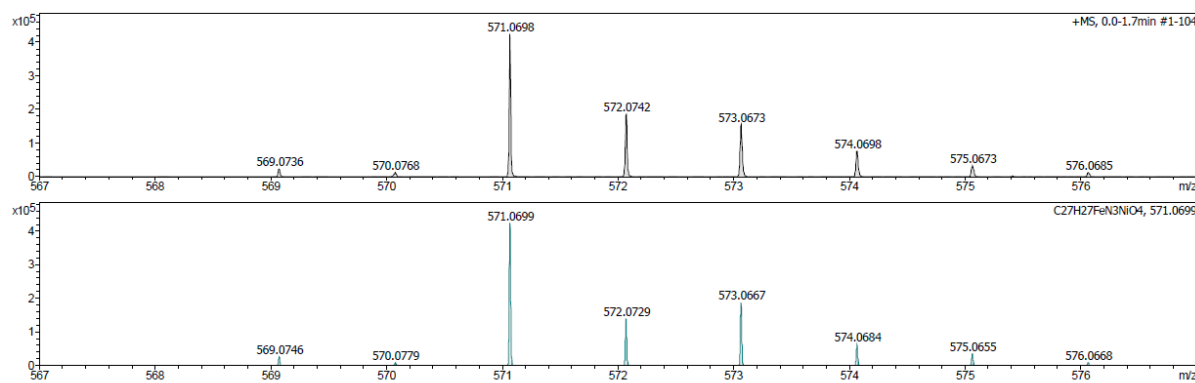


Figure S2. HRMS ESI⁺: experimental (top) and simulated (bottom) ion peaks of the bimetallic complex **3**.

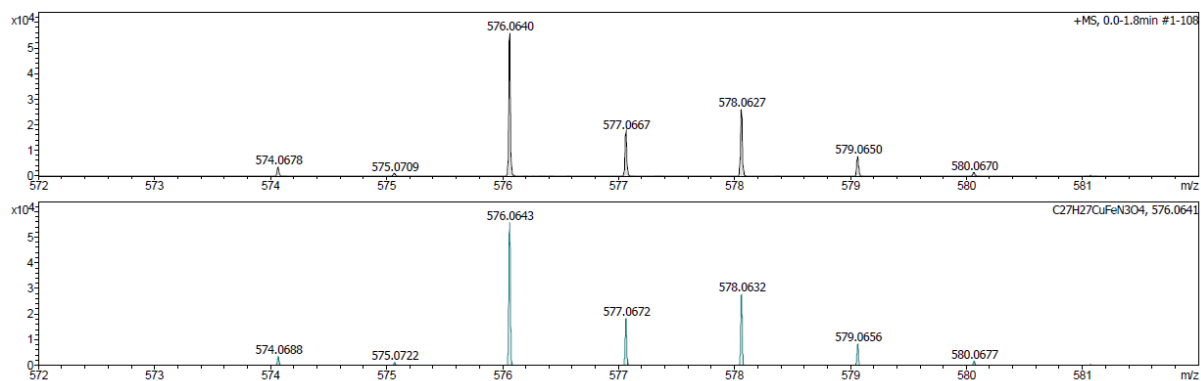


Figure S3. HRMS ESI⁺: experimental (top) and simulated (bottom) ion peaks of the bimetallic complex **4**.

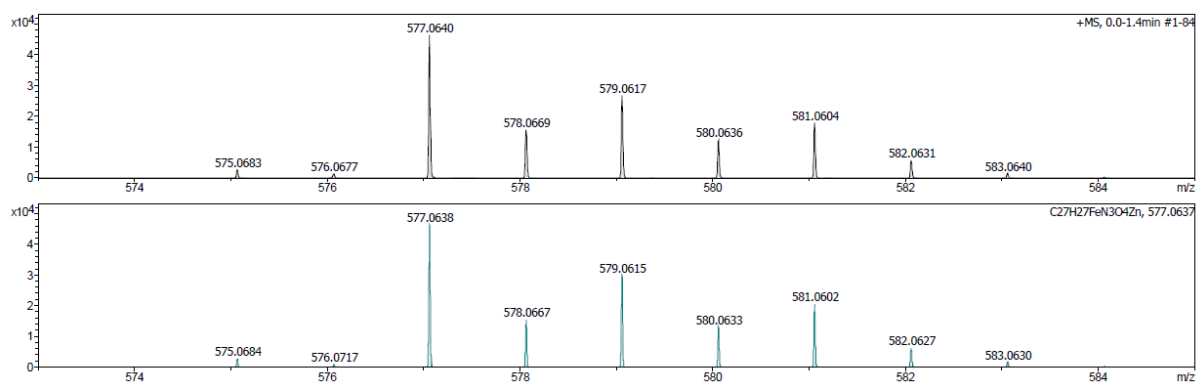


Figure S4. HRMS ESI⁺: experimental (top) and simulated (bottom) ion peaks of the bimetallic complex **5**.

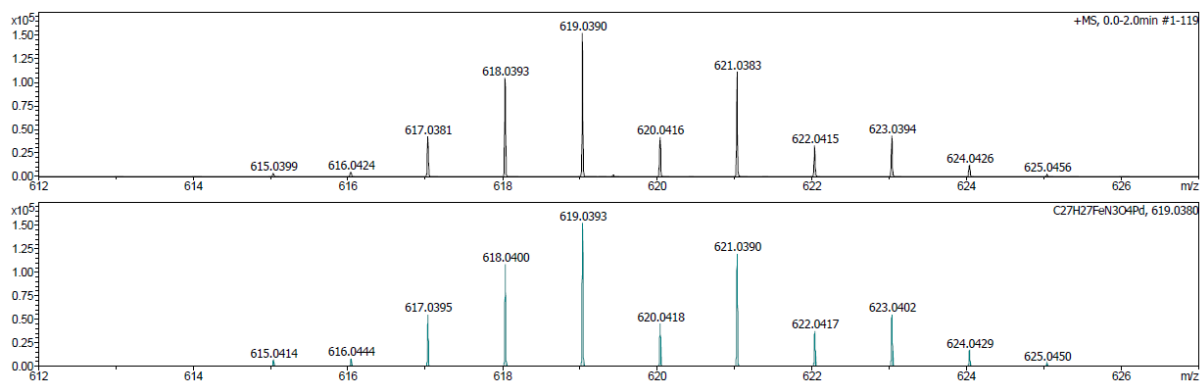


Figure S5. HRMS ESI⁺: experimental (top) and simulated (bottom) ion peaks of the bimetallic complex **6**.

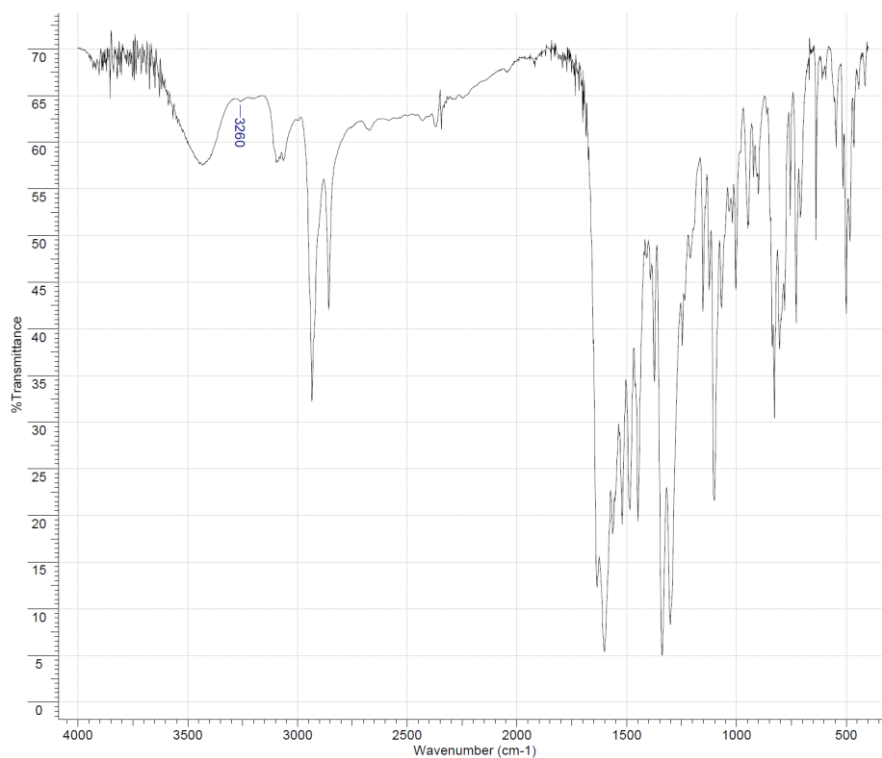


Figure S6. FT-IR solid-state spectrum (KBr disk) of metalloligand **2**.

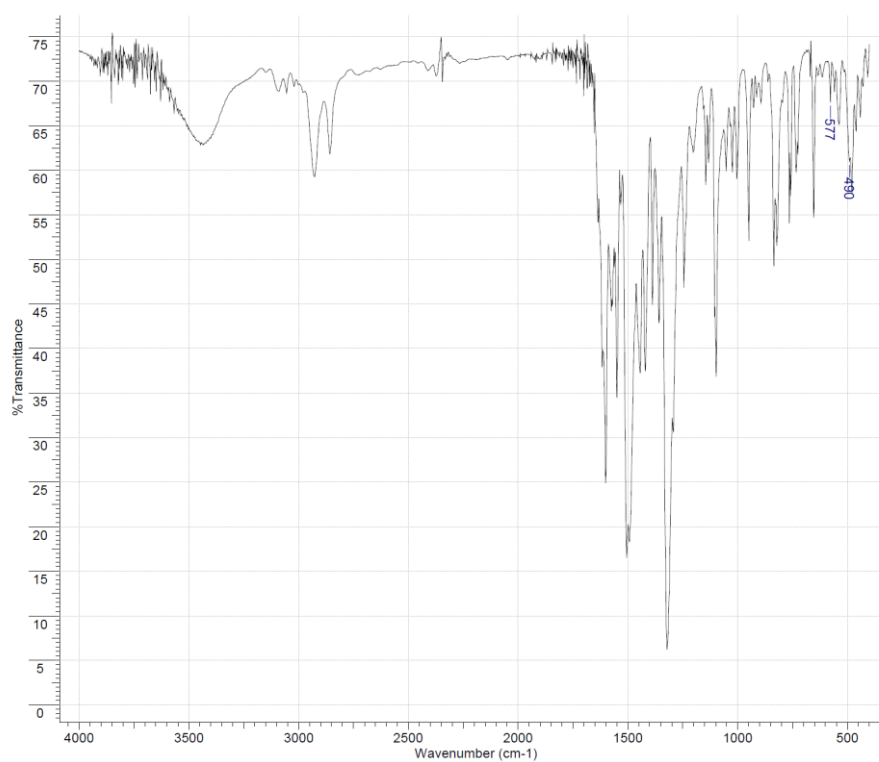


Figure S7. FT-IR solid-state spectrum (KBr disk) of bimetallic complex **3**.

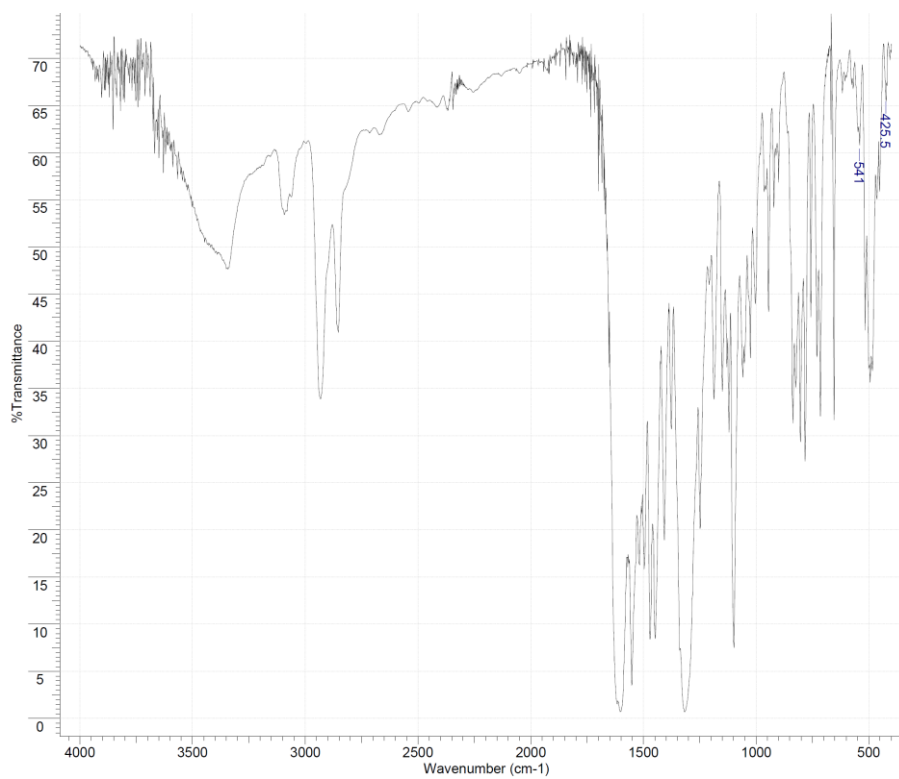


Figure S8. FT-IR solid-state spectrum (KBr disk) of bimetallic complex **4**.

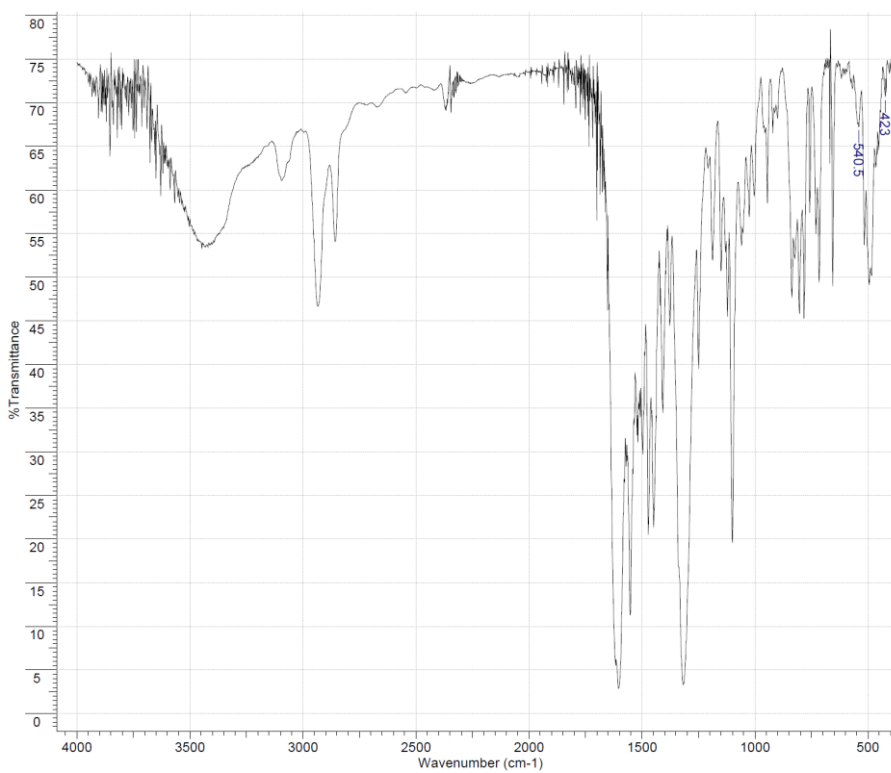


Figure S9. FT-IR solid-state spectrum (KBr disk) of bimetallic complex **5**.

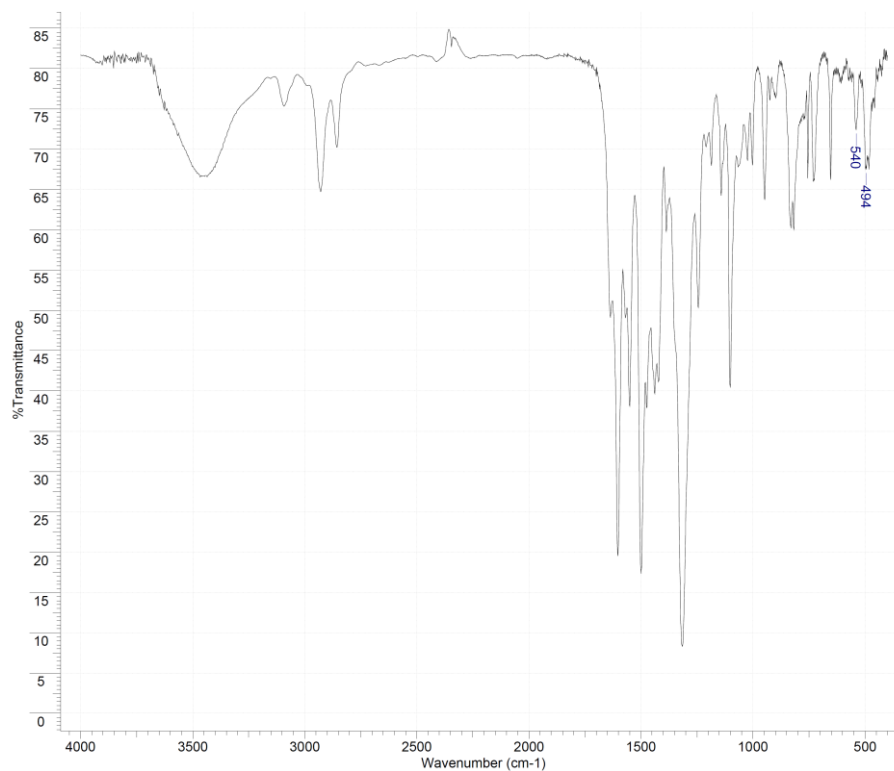


Figure S10. FT-IR solid-state spectrum (KBr disk) of bimetallic complex **6**.

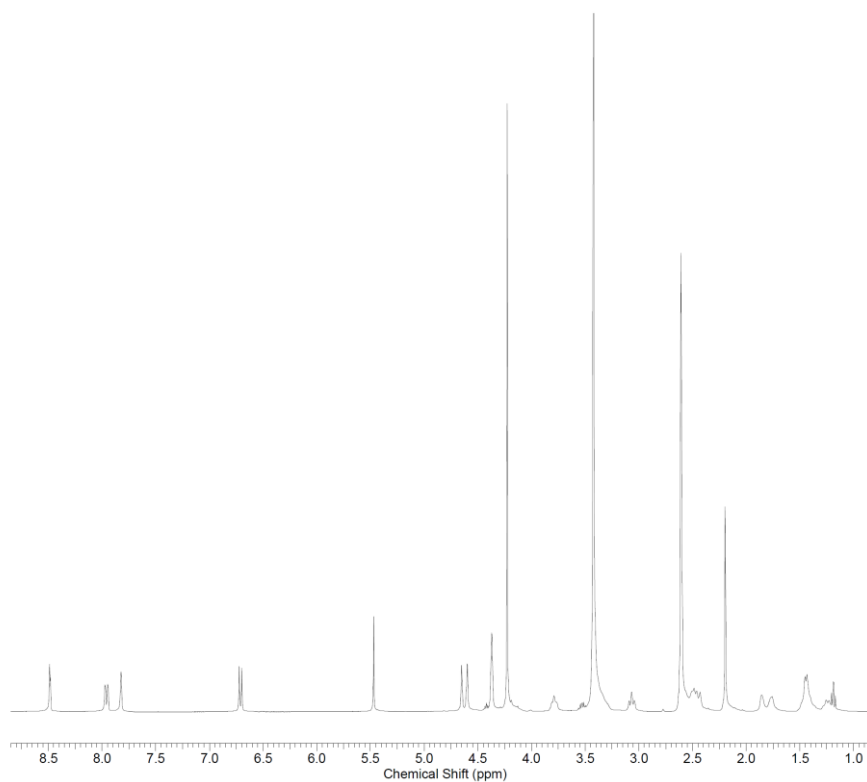


Figure S11. ¹H NMR spectrum of bimetallic complex **3** recorded in DMSO-*d*₆ at 298 K.

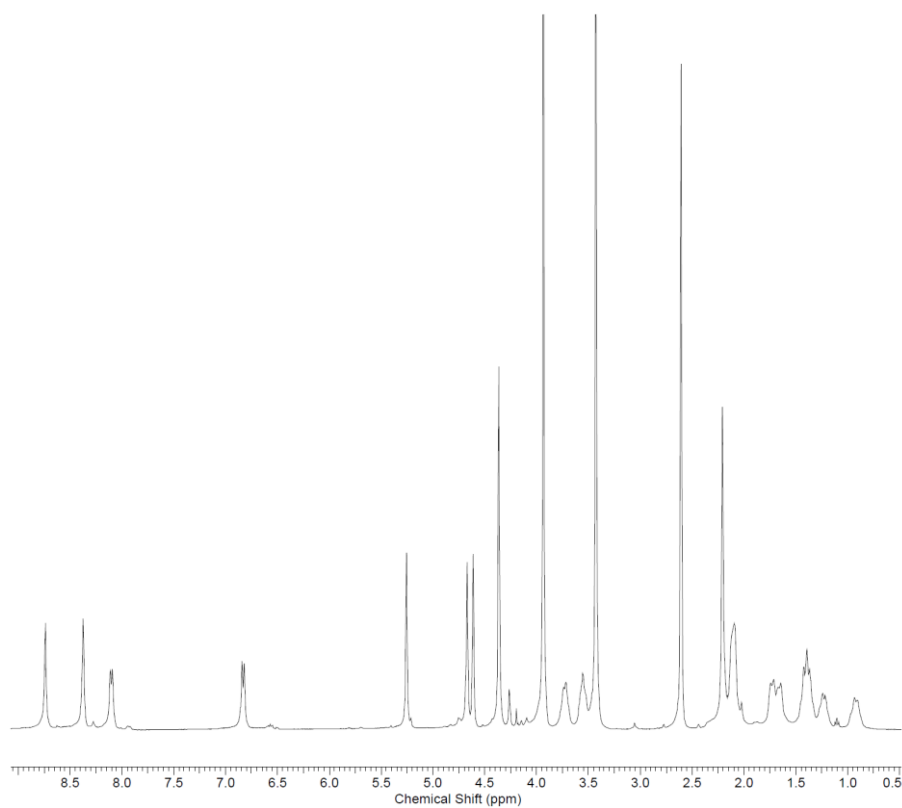


Figure S12. ^1H NMR spectrum of bimetallic complex **5** recorded in $\text{DMSO-}d_6$ at 298 K.

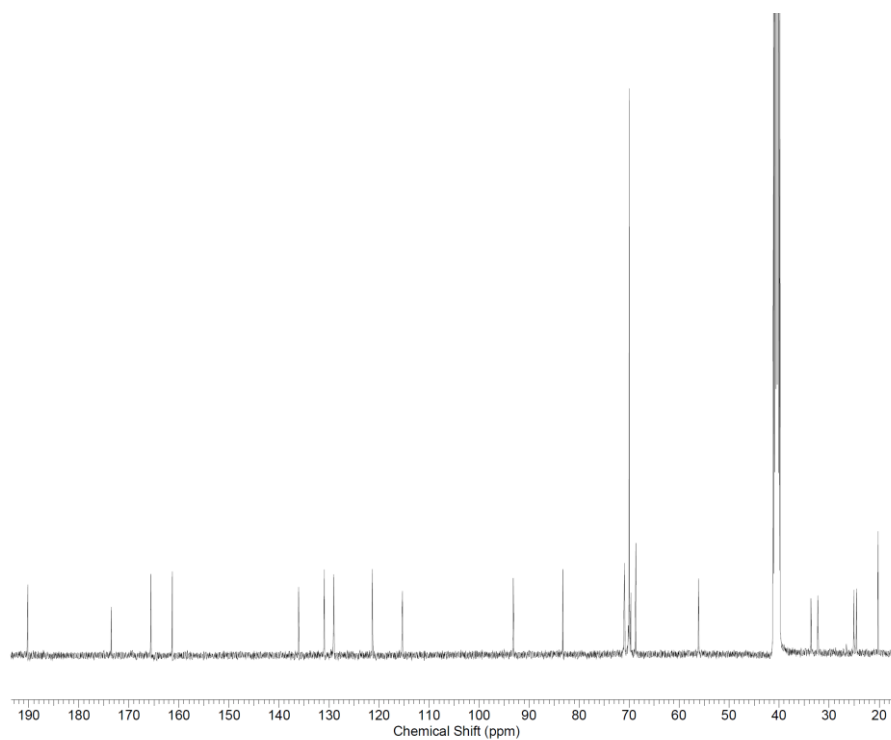


Figure S13. $^{13}\text{C}\{^1\text{H}\}$ NMR spectrum of metalloligand **2** recorded in $\text{DMSO-}d_6$ at 298 K.

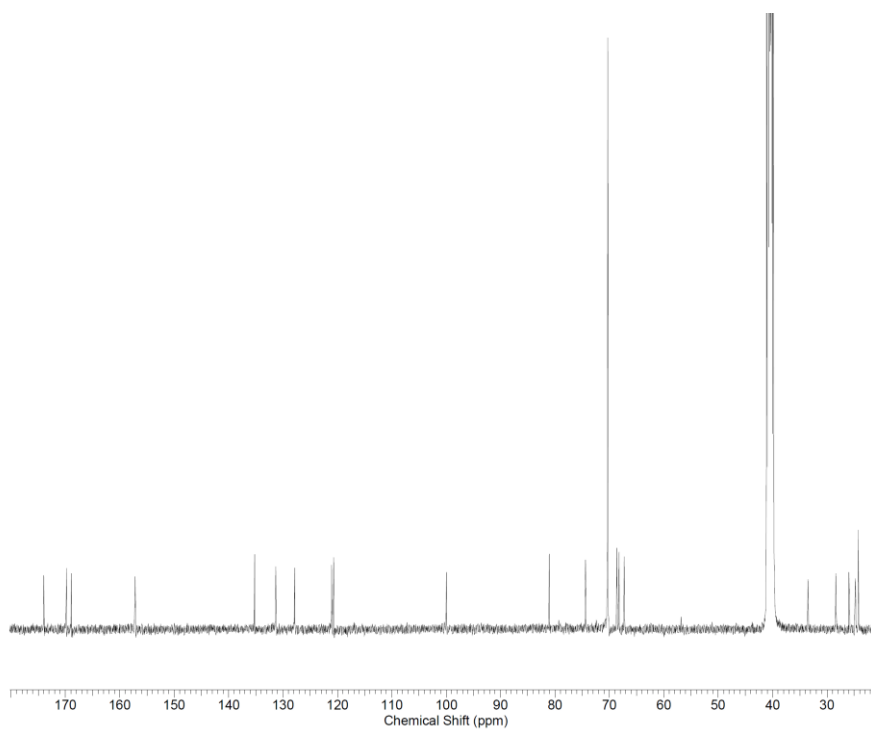


Figure S14. $^{13}\text{C}\{^1\text{H}\}$ NMR spectrum of bimetallic complex **3** recorded in $\text{DMSO-}d_6$ at 298 K.

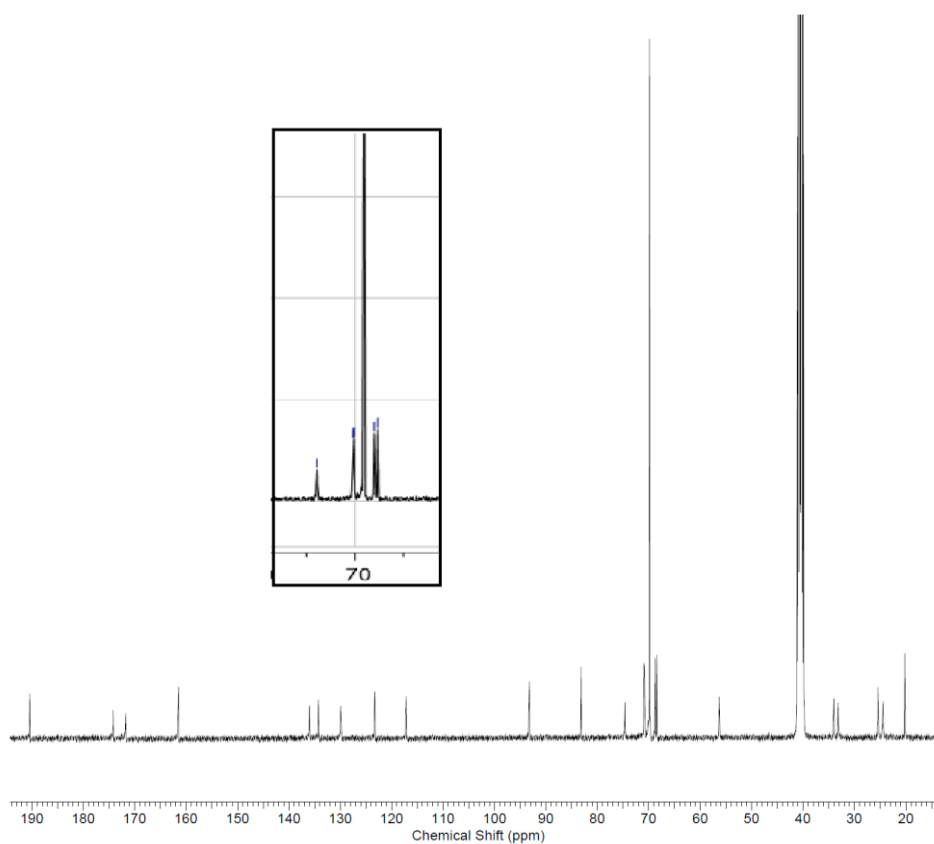


Figure S15. $^{13}\text{C}\{^1\text{H}\}$ NMR spectrum of bimetallic complex **5** recorded in $\text{DMSO-}d_6$ at 298 K.

Inser: resonance pattern of the substituted Cp carbons.

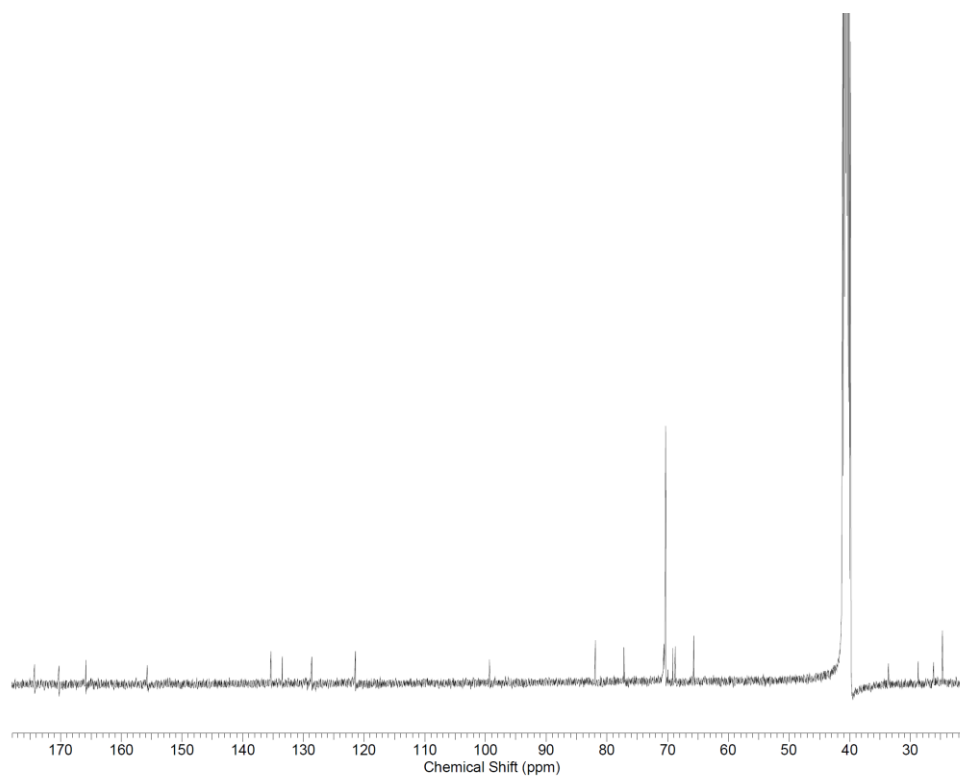


Figure S16. $^{13}\text{C}\{^1\text{H}\}$ NMR spectrum of bimetallic complex **6** recorded in DMSO- d_6 at 298 K.

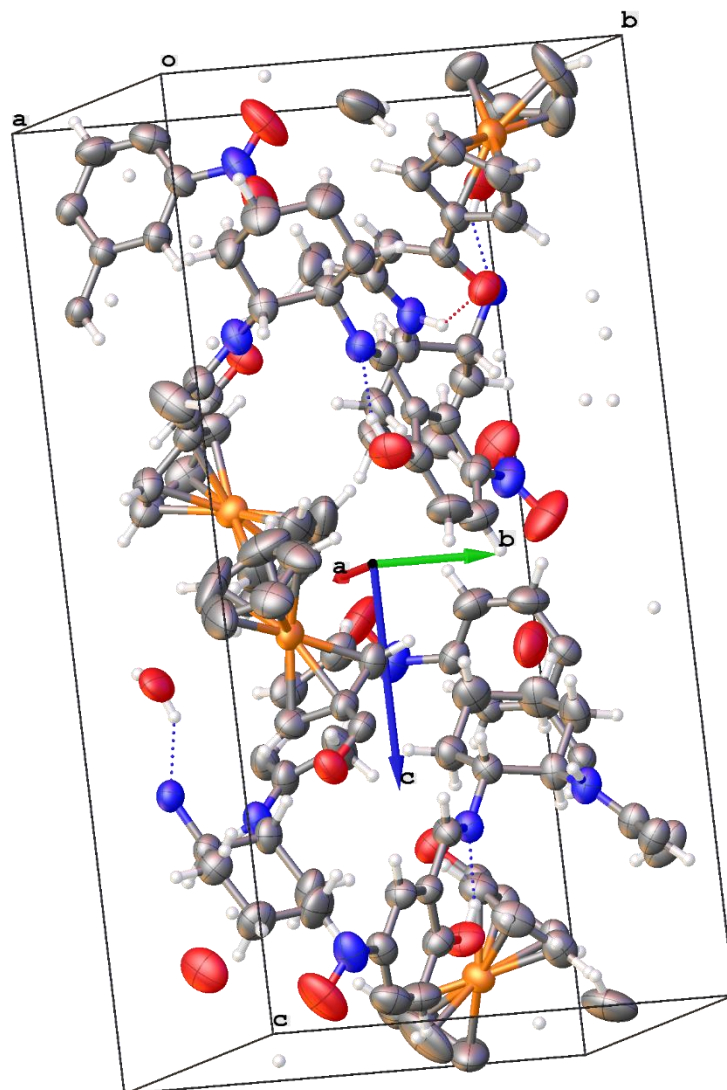


Figure S17. Packing diagram of complex 2 showing the molecular arrangement and hydrogen-bond interactions. Thermal ellipsoids are drawn at 50% probability.

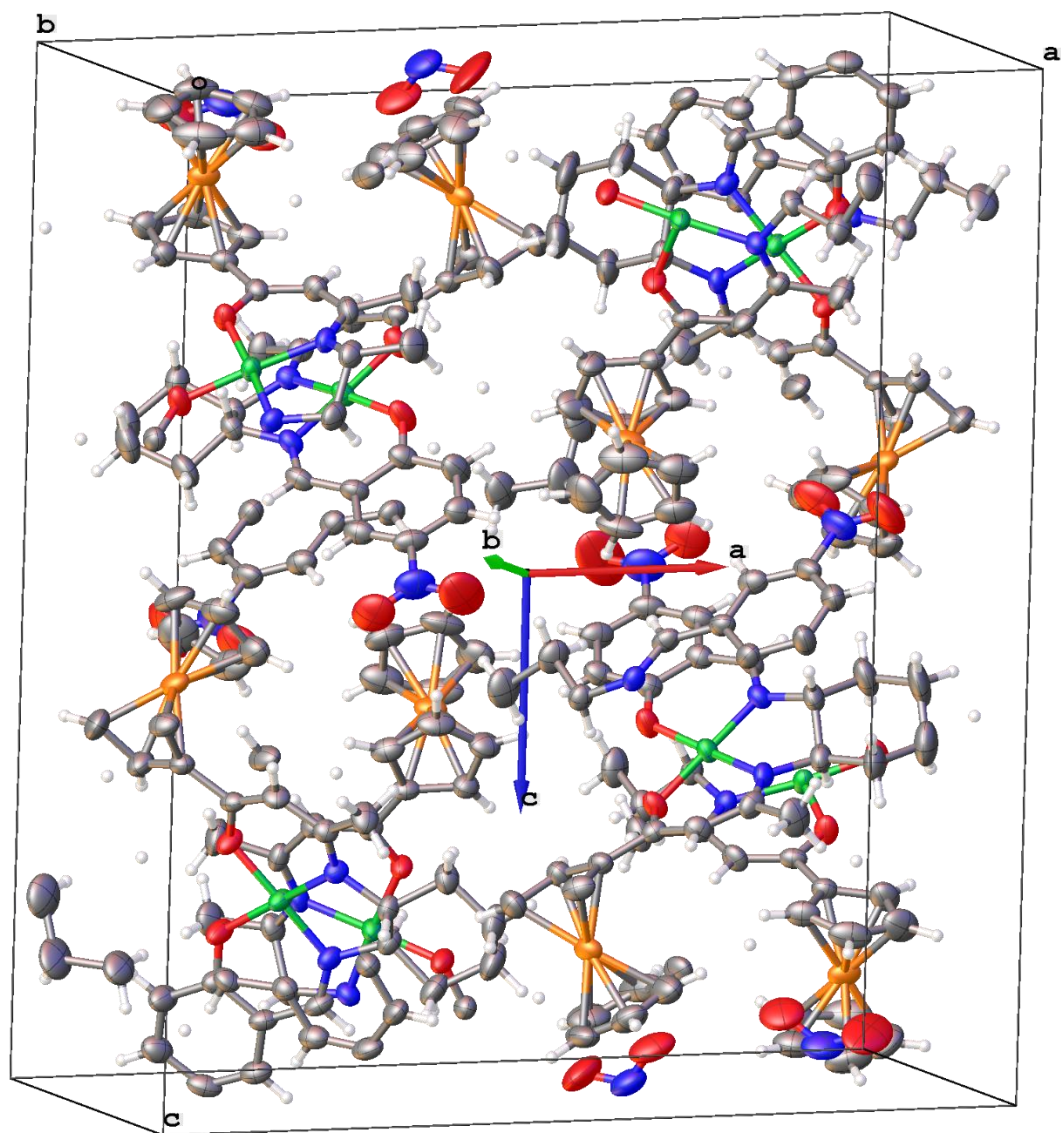


Figure S18. Packing diagram of bimetallic complex **3** showing the molecular arrangement and hydrogen-bond interactions. Thermal ellipsoids are drawn at 50% probability.

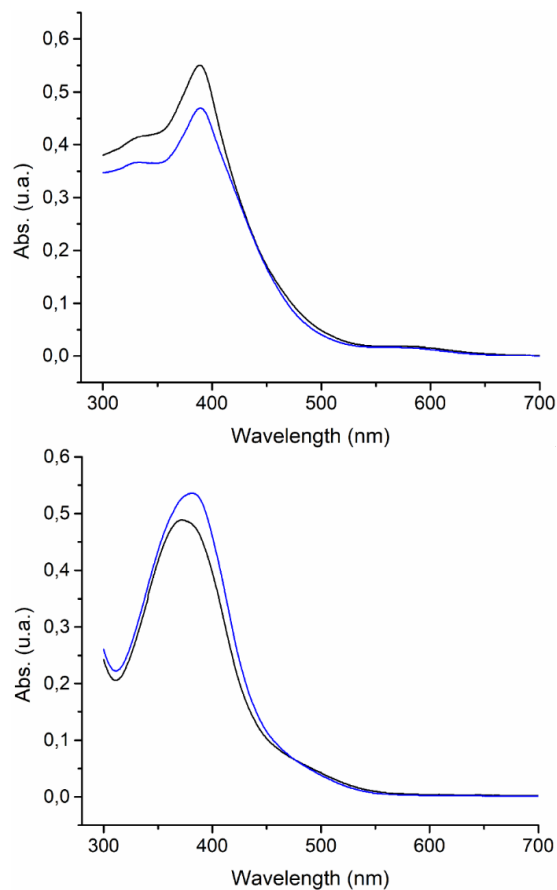


Figure S19. UV-vis spectra of complexes **4** (top) and **5** (bottom) recorded in DCM (black line) and DMF (blue line) solutions.

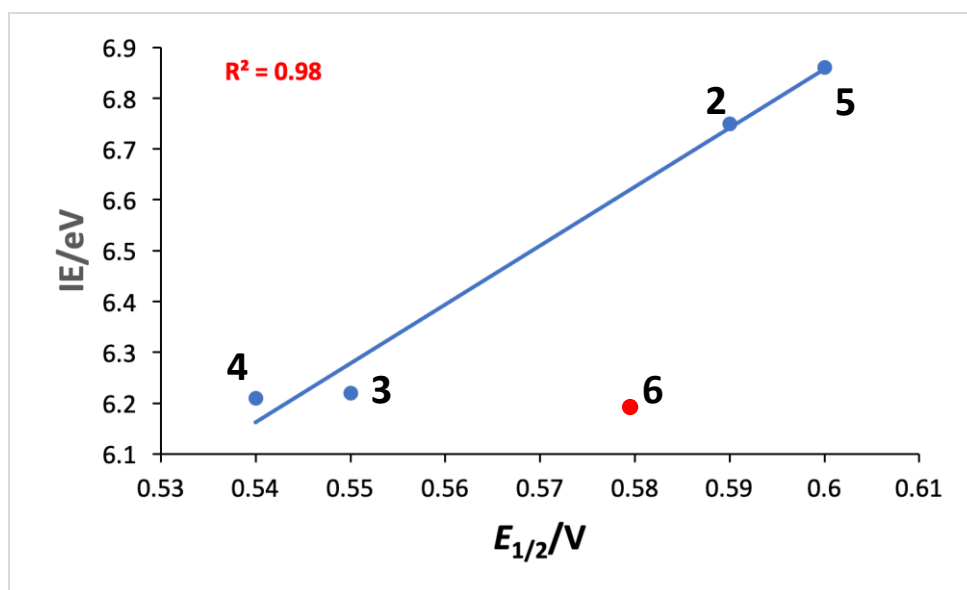


Figure S20. The linear correlation between the electrochemical $E_{1/2}$ and the computed ionization energies of complexes **2**, **3**, **4** and **5**. Complex **6** is added for comparison.

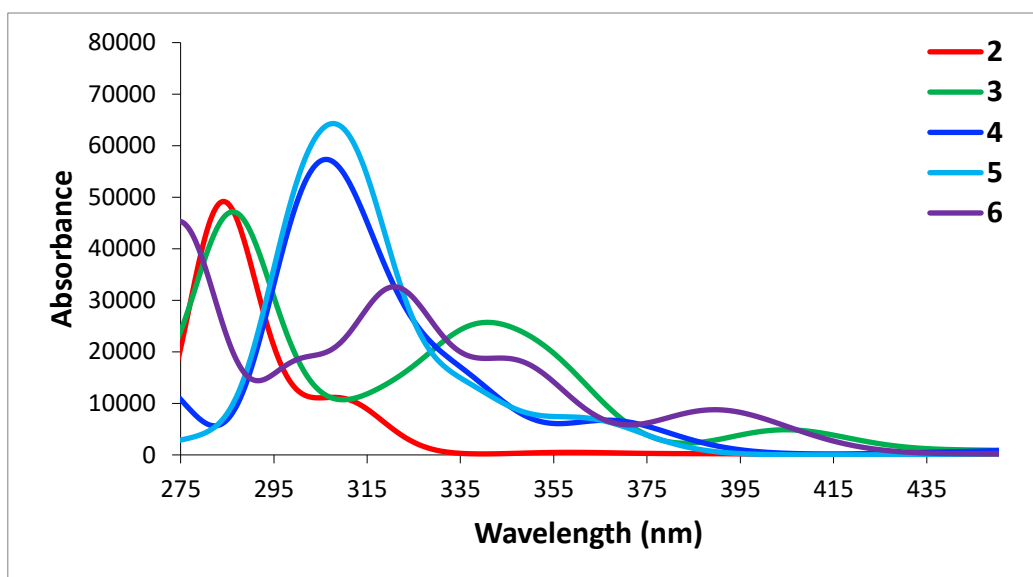


Figure S21. TD-DFT-simulated UV-vis spectra of complexes **2-6**.

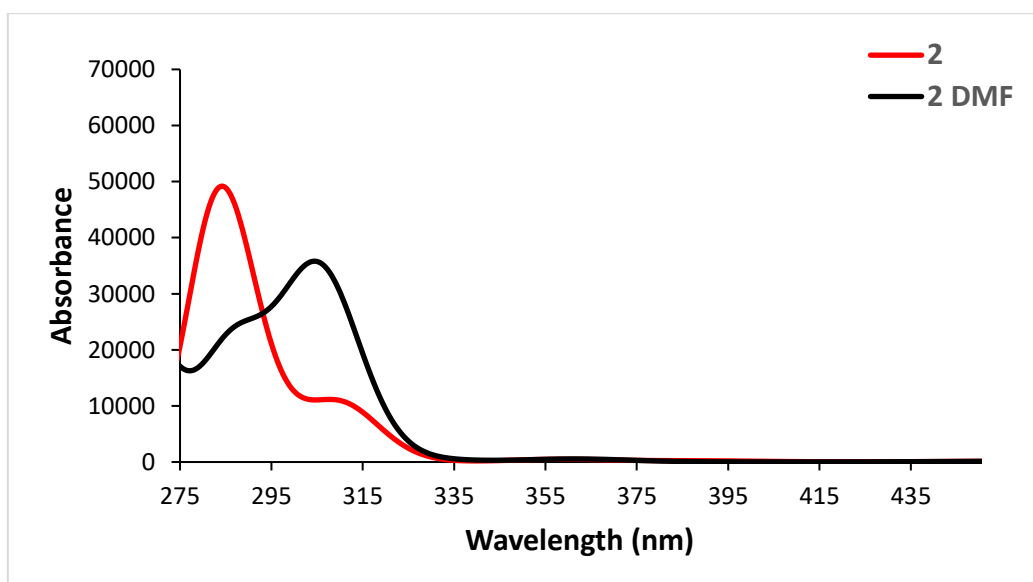


Figure S22. The TD-DFT-simulated UV-vis spectra of complex **2** in vacuum (red curve) and in DMF (black curve).

Table S1. Selected bond distances (Å) and angles (°) for compounds **2** and **3**.

	1	2	3A	3B
Bond distances				
C(11)-O(1)	1.248(4)	1.248(4)	1.284(7)	1.290(7)
C(13)-N(1)	1.321(5)	1.332(4)	1.323(7)	1.309(7)
C(11)-C(12)	1.412(5)	1.411(5)	1.360(9)	1.361(8)
C(12)-C(13)	1.381(5)	1.373(5)	1.414(7)	1.404(8)
N(1)-C(15)	1.468(4)	1.458(4)	1.494(6)	1.492(6)
C(15)-C(16)	1.526(5)	1.538(5)	1.516(6)	1.524(7)
C(16)-N(2)	1.458(6)	1.461(4)	1.478(6)	1.481(6)
N(2)-C(21)	-	1.273(4)	1.287(6)	1.284(7)
C(21)-C(22)	-	1.448(5)	1.446(8)	1.428(7)
C(22)-C(23)	-	1.387(4)	1.421(7)	1.415(7)
O(1)-C(23)	-	1.320(4)	1.287(6)	1.282(6)
C(26)-N(3)	-	1.464(4)	1.447(8)	1.450(8)
N(3)-O(3)	-	1.211(4)	1.212(8)	1.184(9)
N(3)-O(4)	-	1.206(5)	1.204(8)	1.214(8)
Bond angles				
O(1)-C(11)-C(12)	123.7(3)	118.3(3)	124.5(5)	123.3(5)
N(1)-C(13)-C(12)	121.10(3)	121.10(3)	122.40(5)	122.30(5)
C(11)-C(12)-C(13)	123.8(3)	123.9(3)	125.8(5)	126.0(5)
O(2)-C(23)-C(22)	-	121.30(3)	124.00(5)	123.60(5)
N(2)-C(21)-C(22)	-	120.90(3)	124.40(5)	126.00(5)
C(21)-C(22)-C(23)	-	120.20(3)	120.80(5)	121.20(5)
O(3)-N(3)-C(26)	-	117.7(4)	117.8(7)	119.1(8)
O(3)-N(3)-O(4)	-	119.7(3)	122.1(7)	122.0(7)
Ni(1)-O(1)-C(11)	-	-	125.60(4)	124.50(4)
Ni(1)-O(2)-C(23)	-	-	128.20(4)	128.30(3)
Ni(1)-N(1)-C(13)	-	-	122.80(4)	122.70(4)
Ni(1)-N(1)-C(15)	-	-	112.60(3)	108.60(3)
Ni(1)-N(2)-C(16)	-	-	127.70(4)	112.40(3)
Ni(1)-N(2)-C(21)	-	-	127.70(4)	125.50(4)

Table S2. Selected metrical parameters of the ferrocenyl units in compounds **2** and **3**.

Compd	Fe-Cp _{CNT} (Å)	Fe-Cp' _{CNT} (Å)	Cp _{CNT} -Fe-Cp' _{CNT} (°)	Cp/Cp' (°)
2	1.647	1.639	178.5	2.4(4)
3A	1.647	1.650	178.1	10.3(9)
3B	1.658	1.659	179.3	9.3(9)

Abbreviations: Cp = C₅H₅, Cp' = C₅H₄, CNT = centroid.

Table S3. Intra- and intermolecular hydrogen bond interactions in metalloligand **2**.

Natur	D-H...A	D-H (Å)	H...A (Å)	D...A (Å)	∠ D-H...A (°)
Intra	N(1)-H...O(1)	0.86	1.98	2.648(3)	134
Intra	O(2)-H...N(2)	0.82	1.81	2.540(4)	148
Inter	C(2)-h(2A)...O(3) ^{#1}	0.93	2.57	3.433(9)	155
Inter	C(23)-H(23)...O(1) ^{#2}	0.93	2.55	3.345(4)	143
Inter	C(26)-H(26)...O(3) ^{#3}	0.93	2.48	3.206(5)	135

Symmetry transformations used to generate equivalent atoms: #1 = 1/2+x,3/2-y,1-z; #2 = 1-x,1/2+y,1/2-z; #3 = -1/2+x,3/2-y,1-z.

Table S4. Intermolecular hydrogen bond interactions in complex **3**.

D-H...A	D-H (Å)	H...A (Å)	D...A (Å)	∠ D-H...A (°)
C(18A)- H(18A)...O(3A) ^{#1}	0.97	2.42	3.360(9)	164
C(18B)- H(18C)...O(3B) ^{#2}	0.97	2.45	3.341(11)	153

Symmetry transformations used to generate equivalent atoms: #1 = 1/2+x,1/2-y,2-z; #2 = -1/2+x,-1/2-y,2-z.